

SPM-Bench: Benchmarking Large Language Models for Scanning Probe Microscopy

Peiyao Xiao*
Xiaogang Li*
xiaopeiyao.xpy@alibaba-inc.com
lixiaogang.lxg@alibaba-inc.com
Alibaba Group
Beijing, China

Chengliang Xu
Alibaba Group
Beijing, China
xiaodu.xcl@alibaba-inc.com

Jiayi Wang
Skylenage
Beijing, China
denloa975@gmail.com

Ben Wang
Alibaba Group
Beijing, China
yuanjian.wb@alibaba-inc.com

Zichao Chen
Alibaba Group
Beijing, China
chenzichao.czc@alibaba-inc.com

Zeyu Wang
Alibaba Group
Beijing, China
chenfan.wzy@alibaba-inc.com

Kejun Yu
Skylenage
Beijing, China
20170418yu@gmail.com

Yueqian Chen
Skylenage
Beijing, China
yueqianchen1@gmail.com

Xulin Liu
Skylenage
Beijing, China
lxl2691729180@gmail.com

Wende Xiao
Skylenage
Beijing, China
occoo@sina.com

Bing Zhao[†]
Alibaba Group
Beijing, China
xiongdiao@alibaba-inc.com

Hu Wei[†]
Alibaba Group
Beijing, China
kongwang@alibaba-inc.com

Abstract

As LLMs achieved breakthroughs in general reasoning, their proficiency in specialized scientific domains reveals pronounced gaps in existing benchmarks due to data contamination, insufficient complexity, and prohibitive human labor costs. Here we present SPM-Bench, an original, PhD-level multimodal benchmark specifically designed for scanning probe microscopy (SPM). We propose a fully automated data synthesis pipeline that ensures both high authority and low-cost. By employing Anchor-Gated Sieve (AGS) technology, we efficiently extract high-value image-text pairs from arXiv and journal papers published between 2023 and 2025. Through a hybrid cloud-local architecture where VLMs return only spatial coordinates "llbox" for local high-fidelity cropping, our pipeline achieves extreme token savings while maintaining high dataset purity. To accurately and objectively evaluate the performance of the LLMs, we introduce the Strict Imperfection Penalty F1 (SIP-F1) score. This metric not only establishes a rigorous capability hierarchy but also, for the first time, quantifies model "personalities" (Conservative, Aggressive, Gambler, or Wise). By correlating these results with model-reported confidence and perceived difficulty, we expose the true reasoning boundaries of current AI in complex physical scenarios. These insights establish SPM-Bench as a generalizable paradigm for automated scientific data synthesis.

Keywords

Scientific Benchmarking; Automated Data Synthesis; AI for Science; Scanning Probe Microscopy; Multimodal Large Language Model

1 Introduction

Multimodal Large Language Models (MLLM) have demonstrated significant potential in interpreting scientific literature and experimental data across various domains [1, 3, 11, 34, 38]. However, while general-purpose models excel at common reasoning tasks, their proficiency in highly specialized vertical fields—specifically surface physics remains an open question. In this niche, the interpretation of Scanning Probe Microscopy (SPM) images, including Scanning Tunneling Microscopy (STM) and Atomic Force Microscopy (AFM), Transmission Electron Microscopy (TEM) and Scanning Electron Microscopy (SEM), requires more than simple pattern recognition; it demands a doctoral-level understanding of local density of states (LDOS), electronic transitions, and atomic-scale dynamics.

The evaluation of Multimodal Large Language Models (MLLMs) has undergone a paradigmatic shift from general knowledge retrieval [14, 39] to specialized scientific reasoning [13, 36]. While contemporary benchmarks like OlympiadBench and SciBench have pushed the boundaries of university-level STEM problems [4, 7, 9, 10, 31], they predominantly target classical domains such as kinematics or basic chemistry. In the specialized field of surface physics, existing efforts like PhysReason [37] and PHYX [24] lack the high-dimensional expertise required to interpret Scanning Probe Microscopy (SPM) data. Consequently, evaluating MLLMs in such

*Both authors contributed equally to this research.

[†]Corresponding Author

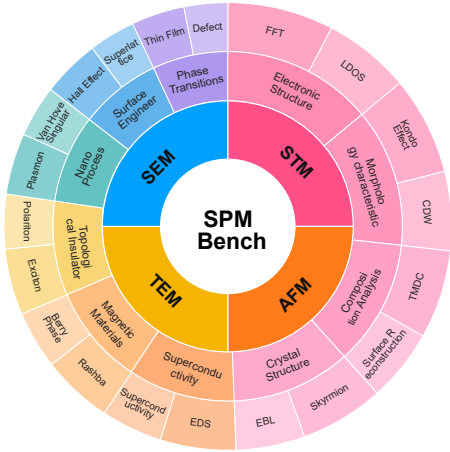


Figure 1: Distribution of SPM-Bench.

Table 1: Key Statistics of SPM-Bench.

Statistic	Number
Total questions	2703
– arXiv paper	407
– Journal paper	418
Unique images	2703
Transmission Electron Microscopy (TEM)	955
Scanning Tunneling Microscopy (STM)	752
Scanning Electron Microscopy (SEM)	558
Atomic Force Microscopy (AFM)	438
Average prompt tokens	3393.4
Average output tokens	1266.0
Average question length	804.7

frontier scientific domains faces an inherent "Scientific Benchmarking Trilemma":

- **Expertise vs. Scalability:** PhD-level benchmarks like SuperG-PQA [5] rely on manual curation by subject-matter experts, rendering them prohibitively expensive and difficult to scale.
- **Purity vs. Contamination:** As models are trained on increasingly vast internet corpora, "stale" benchmarks are inevitably ingested, leading to rampant data contamination and inflated performance.
- **Precision vs. Robustness:** Traditional metrics such as Exact Match (EM) or standard F1-scores are ill-equipped for complex multi-select questions, as they remain vulnerable to speculative "gaming" behaviors.

Despite the emergence of high-quality benchmarks like MatQnA [30] and HLE [23], none simultaneously resolve this trilemma for the SPM domain. There remains a critical need for a benchmark that provides automated expert-level distillation, rigorous temporal separation to ensure data purity, and an evaluation framework robust against speculative reasoning.

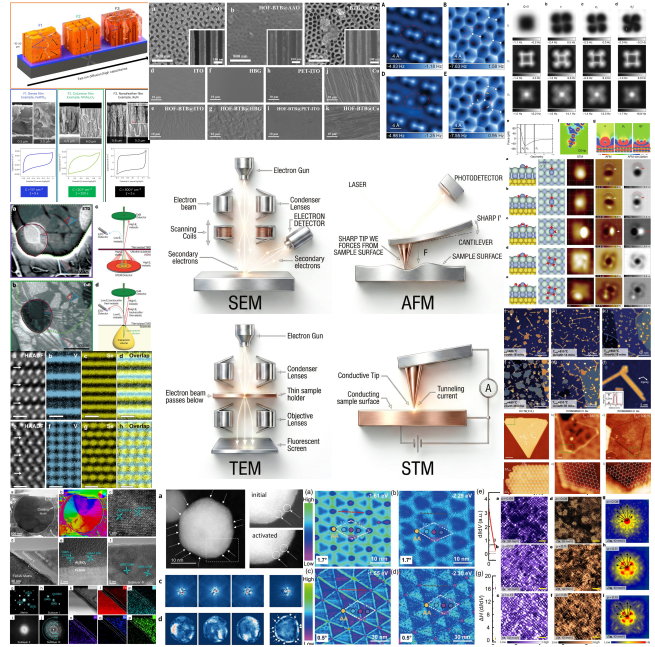


Figure 2: Representative question figures in SPM-Bench.

To bridge these gaps, we present SPM-Bench. Unlike previous works, we construct a fully automated, near-zero-human-intervention pipeline. Our strategy integrates AGS technology with an *llbox*-guided precision cropping mechanism to eliminate 'contextual overload' from complex PDF layouts, delivering distraction-free visual inputs with maximized informational density. Most importantly, we introduce the Strict Imperfection Penalty F1 (SIP-F1) score. This metric rigorously punishes speculative behavior.

The contribution of this work is evident, addressing the critical bottlenecks in domain-specific data synthesis. Our primary contributions are summarized as follows:

Bench for Scanning Probe Microscopy We propose an automated Knowledge Discovery and Refinement Pipeline designed for high-value scientific literature. This framework transforms raw, unstructured physical science corpora into a high-entropy, expert-level multimodal benchmark for SPM.

High-Fidelity VLM-Guided Segmentation We propose a novel image extraction pipeline that leverages VLMs to perform semantic-aware spatial localization.

Multi-Agent Adversarial Framework We implement a robust data synthesis workflow centered on an Advisory Model refinement loop.

Robust Engineering Workflow We demonstrate a high-throughput engineering pipeline optimized for large-scale data synthesis.

Figure 2 illustrates the multimodal heterogeneity of SPM-BENCH, which spans a spectrum of Scanning Probe (STM, AFM, nc-AFM) and Electron Microscopy (SEM, TEM) domains. Beyond rudimentary visual perception, our benchmark mandates **epistemic grounding** in quantum-mechanical phenomena, including dI/dV spectroscopy and moiré superlattice dynamics. SPM-BENCH uniquely challenges **multi-scale spatial-frequency reasoning**, requiring

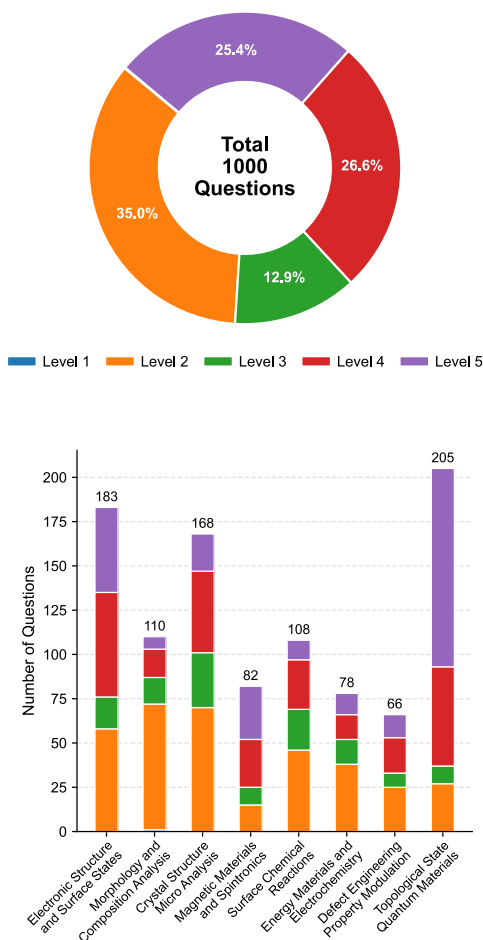


Figure 3: Statistical analysis of question complexity. Upper: stacked bar chart of question frequency. Lower: cognitive level distribution.

models to correlate angstrom-scale structural perturbations with mesoscopic property modulations. By synthesizing experimental datasets with theoretical models and analytical plots, SPM-BENCH transcends perceptual object recognition, necessitating a sophisticated latent understanding of reciprocal-space logic, symmetry breaking, and complex probe-sample interaction physics.

As shown in Bloom’s distribution analysis (Figure 3), while general-purpose benchmarks like *ScienceQA* or *MMMU* are heavily skewed toward Level 1-2 (Recall/Comprehension) [36], SPM-Bench maintains a significantly higher proportion of Level 4-5 questions. This "Research-grade" distribution ensures that the benchmark probes the true reasoning boundaries of current AI agents in the pursuit of doctoral-level scientific discovery.

2 Data Synthesis Pipeline

2.1 Data Acquisition

The SPM-Bench dataset is exclusively curated from over 30 premier physical science journals and the arXiv repository, establishing

a high-fidelity foundation that stands in stark contrast to noisy, general-purpose web-crawled corpora. Our pipeline leverages a "curated-by-experts" strategy: by targeting high-impact journals, we tap into a metadata repository where every figure caption and technical discussion has been refined through multiple rounds of rigorous peer scrutiny. Consequently, these elements serve as gold-standard, expert-verified annotations for multimodal learning [19, 33]. This foundation is synergistically complemented by arXiv preprints, which infuse the dataset with the latest research and frontier methodologies. Such a balance between peer-reviewed reliability and frontier timeliness guarantees a level of "academic purity" and professional depth that is essential for deciphering the complex characterization tasks inherent in the physical sciences.

To handle the massive throughput of physics literature, we implemented a localized pre-processing stage designed to filter redundant information before any model inference occurs.

Anchor-Gated Sieve (AGS) This mechanism performs a local spatial layout analysis, triggering extraction logic only when a page concurrently contains both image blocks (Images/Drawings) and figure caption anchors. By heuristically filtering out over 95% of text-heavy pages, AGS drastically improves processing efficiency and reduces computational overhead. The extraction logic employs a dual-stage heuristic to ensure the "Academic Purity" of the captured data. We utilize a strict, multiline regular expression (e.g., Figure 1, FIG. 1, Extended Data Fig. 1) specifically designed to identify figure headers at the start of text blocks. This prevents citation leakage, where body-text references (e.g., as seen in Fig. 1) are misidentified as actual figure captions.

Token-Saving Pre-segmentation Unlike conventional full-document multimodal recognition [14, 17, 32], our pipeline performs precise image-caption pairing locally. By generating "semantic fingerprints" for localized slices, the system ensures that only high-value visual regions are queued for subsequent processing, reducing latent noise and lowering downstream token consumption by several orders of magnitude.

2.2 Cloud-Local Architecture

The layout of academic figures in physical science literature is notoriously complex, often featuring sub-panels with overlapping labels and tightly-packed captions. Traditional computer vision techniques, such as Canny edge detection [2] or Hough transforms [6], frequently fail to distinguish between graphical boundaries and textual annotations. This limitation has been long recognized in the field of document analysis, where separating text from mixed graphics remains a challenge due to their overlapping low-level features [8, 27]. Furthermore, simple structural analysis often lacks the semantic context necessary to correctly interpret complex layouts [22]. Our approach utilizes the deep semantic understanding of VLMs to interpret the spatial hierarchy of the page. By instructing the model to generate a unified bounding box strictly for visual panels, we achieve a "clean" decoupling of data from description. This ensures that the resulting dataset tests the model’s ability to interpret visual evidence rather than its ability to read local textual cues, thus preventing further data leakage.

Besides, from a computer engineering perspective, transferring high-resolution (300+ DPI) images directly to cloud-based APIs is

SPM-Bench Automated Data Synthesis and Evaluation Pipeline

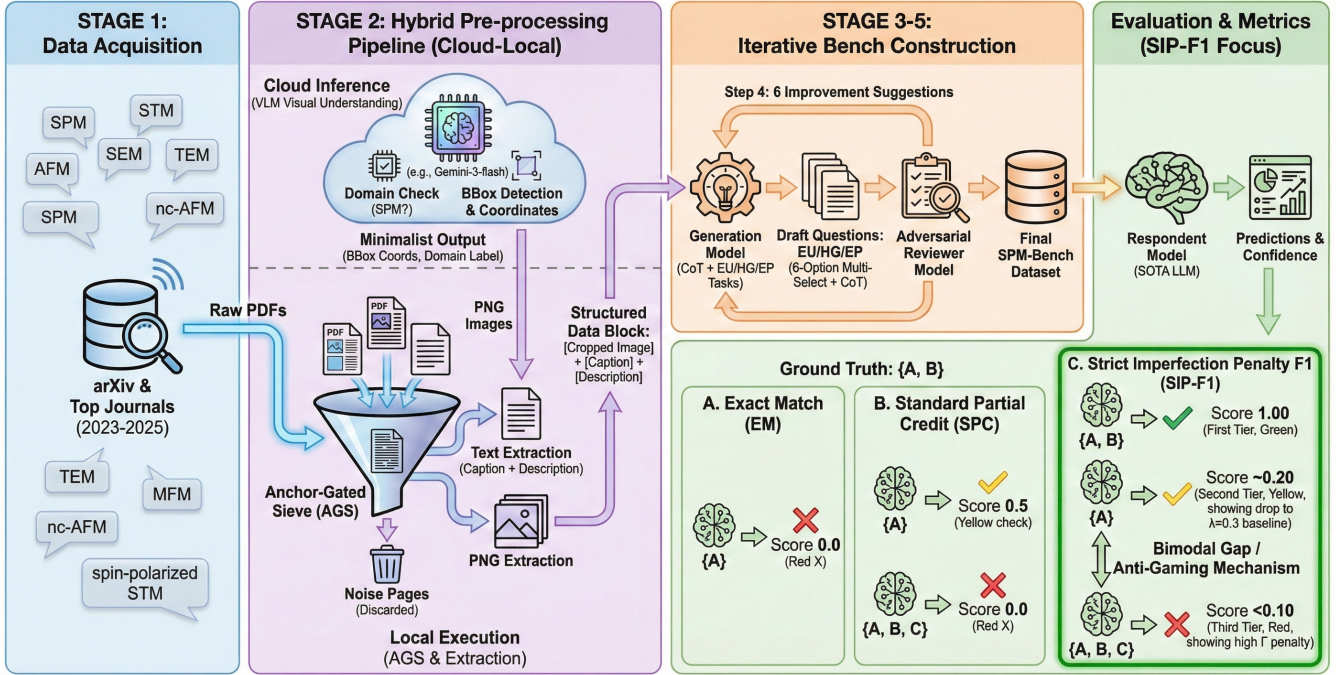


Figure 4: Overview of the data synthesis pipeline in SPM-Bench.

both cost-prohibitive and latency-heavy. Our pipeline implements an Adaptive Resolution Strategy. One is **remote contextual inference**: High-resolution PNGs are downsampled to a 1024-pixel thumbnail before being encoded for VLM processing. This reduces the input token count by approximately 70 percent without sacrificing the model’s ability to identify spatial coordinates. The other is **local high-fidelity execution**: The VLM returns normalized coordinates [0, 1000], which our local engine maps back to the original high-resolution canvas for the physical crop. This "remote inference, local execution" paradigm ensures that the synthesized sub-figures retain their sub-pixel clarity for subsequent training or evaluation phases.

Extreme Token Efficiency The pipeline restricts VLM outputs exclusively to four-dimensional spatial coordinates and modality labels, deliberately avoiding the generation of costly descriptive text. This "minimalist output" strategy reduces API expenditure by over 90%, demonstrating superior cost-effectiveness for large-scale scientific data mining.

Physical Feature Pre-filter Instead of brute-force rendering, the pipeline implements a physical-feature pre-filter to minimize computational overhead. First, physical filtering is used for each page, the system queries the PDF internal object tree using PyMuPDF get images and get drawings methods. Pages devoid of graphical objects or those containing fewer than 12 vector drawing primitives are discarded, effectively skipping text-only pages without full-page rendering. Next, high-fidelity rasterization is applied to preserve the sub-pixel details required for microscopic characterization, candidate pages are rendered using a coordinate transformation matrix,

where the zoom factor is dynamically calculated to achieve a target density of 300 DPI (standardized from the 72-point PDF coordinate system). This ensures that the local PNG snapshots retain sufficient clarity for secondary LLM-based sub-figure segmentation.

Information Density Control To ensure high-quality evaluation queries, a structural richness threshold is enforced. The pipeline exclusively selects complex figures containing at least four sub-panels (e.g., microscopy images coupled with corresponding spectroscopy), guaranteeing that the curated assets possess sufficient informational density for advanced scientific reasoning.

2.3 Question and Answer Generation

Utilizing structured outputs from the above AGS and local PyMuPDF captures, the engine precision-feeds the VLM (gemini-3-flash-preview) with three distinct streams of information: (1) **Visual Evidence**: High-resolution local crops of SPM topography, atomic-scale lattices, or spectroscopic mappings. (2) **Intellectual Provenance**: High-value discussion snippets containing the original authors’ complex physical interpretations and causal logic. (3) **Scientific Constraints**: Domain-specific technical libraries (TECH-LIB) and analytical frameworks (ANALYSIS-LIB) to enforce the use of precise terminology (e.g., moiré superlattices, LDOS mapping).

By narrowing the model’s focus to these expert-verified snippets, we achieve "Knowledge Densification." This allows the VLM to generate questions of extreme complexity without the prohibitive token cost and "distractor noise" associated with processing entire manuscripts. To elevate the output quality from descriptive to analytical, we implemented a self-reflective architecture for generating

question. This mandates the generation of two critical cognitive scaffolds, namely the CoT and rubric engineering, which can act as a quality-control dimension for each question.

De-noising The question generator model gemini-3 are given the llbox figure, figure caption and figure discussions. By narrowing the model’s focus to these expert-verified caption and discussions, we achieve high-quality, figure-aligned prerequisite knowledge.

CoT Reasoning Before finalizing the question stem, the model is required to articulate a hidden reasoning path [21, 26, 28, 29, 35]. This internal dialogue forces the VLM to synthesize the figure’s visual features with the expert discussion’s physical laws (e.g., correlating a height profile dip with a specific stacking order). This step acts as a **logical anchor**, ensuring high internal consistency between the image and the question.

Rubrics The model must simultaneously define a set of scoring criteria [18, 20]. By forcing the generator to “think like an examiner,” it inherently raises the bar for the question’s complexity [25]. These rubrics target specific PhD-level competencies, such as “Symmetry Breaking Identification” or “Experimental Parameter Sensitivity,” transforming the VLM from a passive respondent into an active scientific instructor.

Concurrency To handle the synthesis of tens of thousands of records, our architecture employs a hybrid parallelism model. We utilize ProcessPoolExecutor for CPU-intensive PDF parsing and ThreadPoolExecutor for IO-bound API communications. To ensure system reliability, we implemented Atomic Persistence: processed records are immediately synchronized to the disk in a structured JSON format. Coupled with a hash-based deduplication mechanism, this provides the system with robust “warm-restart” capabilities, allowing for seamless recovery from network interruptions or API rate-limiting without data loss.

2.4 Adversarial Optimization

To bridge the gap between “machine-generated” and “expert-level” questions, we introduce an Advisory Model into the synthesis loop. This agent performs a multi-criteria audit of each Q&A pair, evaluating parameters such as scientific consistency, distractor plausibility, and logical depth. By forcing the generator to iterate based on these six-dimensional critiques, we significantly increase the cognitive load of the benchmark. This adversarial process effectively mitigates the common “shallow-pattern-matching” bias found in many synthetic datasets.

3 Evaluation Metrics

To comprehensively evaluate the reasoning ability and robustness of Large Language Models (LLMs) on multi-modal multi-select questions, this study adopts three scoring paradigms with different granularities for comparative analysis: Exact Match (Baseline Metric), Standard Partial Credit (Traditional Educational Metric), and the proposed Strict Imperfection Penalty F1 (High-Robustness Evaluation Metric).

3.1 Exact Match (EM)

Exact Match is the most fundamental evaluation metric in machine learning tasks. This metric requires that the model’s predicted results must be completely consistent with the ground truth; any

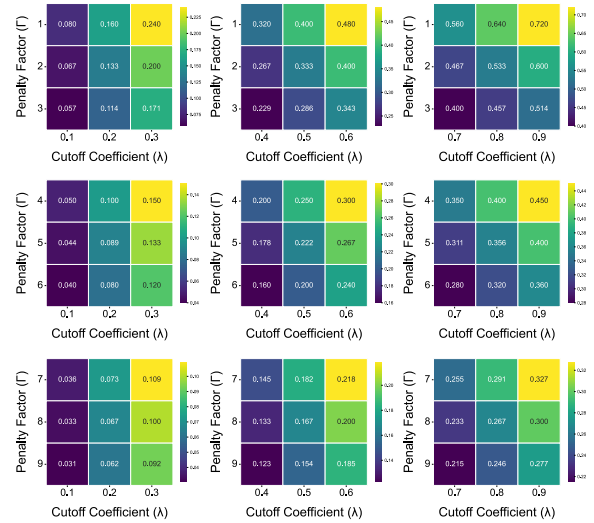


Figure 5: Parametric sensitivity of the SIP-F1 metric.

form of under-selection, over-selection, or incorrect selection is considered an error.

Definition Formula (Assuming a maximum score of 1.0 per question):

$$\text{Score}_{EM} = \begin{cases} 1.0 & \text{if } S_{\text{model}} = S_{\text{correct}} \\ 0.0 & \text{otherwise} \end{cases} \quad (1)$$

Feature Analysis This metric measures the Absolute Accuracy of the model. However, in multi-modal reasoning tasks, this metric is overly strict. It cannot distinguish between “completely wrong” models and “partially correct” models, losing fine-grained information regarding the model’s reasoning boundaries and easily masking the partial reasoning capabilities of models in complex scenarios.

3.2 Standard Partial Credit (SPC)

This metric refines the traditional educational scoring logic by adopting a **proportional scoring mechanism**. Unlike the binary Exact Match (EM) metric, SPC acknowledges the model’s partial mastery of knowledge. It awards credit based on the proportion of correctly identified options (Recall), strictly under the condition that **no incorrect options** are selected (i.e., Precision must be 1.0). The core principle remains “Encourage Conservatism, Punish Errors”. If the model selects a proper subset of the correct answer (under-selection), the score is calculated as the ratio of hit options to the total number of correct options. However, once any incorrect option is included—regardless of how many correct ones are found—the score is strictly judged as zero.

Definition Formula

$$\text{Score}_{SPC} = \begin{cases} 1.0 & \text{if } S_{\text{model}} = S_{\text{correct}} \\ \frac{|S_{\text{model}}|}{|S_{\text{correct}}|} & \text{if } S_{\text{model}} \subset S_{\text{correct}} \text{ (Proper Subset)} \\ 0.0 & \text{otherwise} \end{cases} \quad (2)$$

Feature Analysis By introducing proportional scoring, SPC addresses the granularity issue of fixed-score metrics. It effectively

measures the model’s “Pure Recall” capability under a zero-tolerance constraint for hallucinations. While fairer than EM, its immediate drop to zero upon a single error ensures that the model is not rewarded for “lucky guesses” mixed with misinformation.

3.3 Strict Imperfection Penalty F1 (SIP-F1)

Background and Motivation To address the deficiencies of the aforementioned metrics in terms of granularity and anti-interference, this study proposes the SIP-F1 metric, which is an improvement based on the F1-Score. Traditional F1 metrics often lack discrimination due to awarding overly high scores for “under-selection strategies” (e.g., 0.67). SIP-F1 introduces a two-stage gating mechanism and dynamic penalty coefficients to impose a devastating strike on speculative “select all” or “random selection” behaviors while measuring Recall, aiming to implement a “Perfectionism” orientation in evaluation.

- **Perfect Gating** The score is 1.0 only when the model output is completely consistent with the standard answer.
- **Imperfection Penalty** Once any flaw exists in the output, the score baseline is immediately lowered to λ (the cutoff coefficient, set to 0.6 in this study). Based on this reduced weight, a high-penalty Asym-F1 algorithm is applied to ensure that the score for “under-selection” is superior to “over-selection/wrong selection.”

Definition Formula

$$\text{Score} = \begin{cases} 1.0 & \text{if } S_{\text{model}} = S_{\text{correct}} \\ \lambda \times \text{Score}_{\text{F1-Gamma}} & \text{otherwise} \end{cases} \quad (3)$$

$$P_w = \frac{TP}{TP + (FP \times \Gamma)}, \quad R = \frac{TP}{|S_{\text{correct}}|} \quad (4)$$

$$\text{Score}_{\text{F1-Gamma}} = 2 \times \frac{P_w \times R}{P_w + R} \quad (5)$$

Note: TP is the number of True Positives, FP is the number of False Positives. The parameters are set as $\lambda = 0.6$ and $\Gamma = 6$ based on a pilot study, as shown in Table 4, to ensure that any hallucinated or incorrect option leads to a final score lower than the most conservative, correct partial answer.

- **First Tier (1.00)** Completely correct. Only models with extremely high reasoning capabilities gather in this region.
- **Second Tier (~0.40)** Conservative response. The model acknowledges knowledge boundaries and produces no hallucinations. Although penalized, the score is significantly higher than blind guessing.
- **Third Tier (<0.25)** Aggressive response. Due to the penalty of $\Gamma = 6$, any answer containing incorrect options will score lower than a conservative response, even if all correct items are found.

High Discrimination and Bimodal Effect By introducing SIP-F1, we found that the model score distribution presents a significant Bimodal Distribution: models with expert-level capabilities gather near 1.0, while the scores of any model attempting to speculate or possessing only partial knowledge are suppressed below 0.6. This draws an insurmountable gap between perfect models and flawed models.

Strong Robustness and Anti-Gaming Mechanism SIP-F1 has a natural inhibitory effect against the speculative behavior of large models tending to “list all options” to gain recall scores (Gaming the Metric), as shown in Table 2. As FP (incorrect options) increases, the Γ coefficient multiplies its impact on the denominator, causing precision to drop sharply. For “select-all parties,” the final score will approach zero, forcing the model to pursue precise reasoning.

Figure 5 illustrates the SIP-F1 scores for the Aggressive strategy ($TP = 2, FP = 1$) under varying combinations of the cutoff coefficient λ and the penalty factor Γ . As shown, the score decreases monotonically with increasing Γ for any fixed λ , confirming the penalty factor’s effectiveness in suppressing hallucinated outputs. Across a broad parameter region ($\lambda \in [0.4, 0.7]$, $\Gamma \in [4, 8]$), the Aggressive-strategy score remains consistently below the Conservative-strategy score (0.40), indicating that the desired ranking is structurally stable rather than sensitive to a specific parameter choice. The adopted setting of $\lambda = 0.6, \Gamma = 6$ achieves an effective balance between penalizing incorrect selections and preserving a meaningful scoring gradient among partially correct responses.

Using the metric, the results clearly value orientation and scoring ladder: the indicator successfully constructs a strict scoring hierarchy, effectively widening the gap between perfect models and mediocre models:

Table 2: Performance Comparison: EM vs. SPC vs. SIP-F1.

Personality	Choices	Intermediate Stats				Metric Scores		
		TP	FP	R	P_w	EM	SPC	SIP
Comprehensive	{A, B}	2	0	1.0	1.00	1.00	1.00	1.00
Conservative	{A}	1	0	0.5	1.00	0.00	0.50	0.40
Aggressive	{A, B, C}	2	1	1.0	0.25	0.00	0.00	0.24
Gambling	{A, B, C, D}	2	2	1.0	0.14	0.00	0.00	0.15

4 Results

4.1 Comparative Analysis

Figure 7 provides a granular decomposition of model performance across three distinct evaluation paradigms: Exact Match (EM), Standard Partial Credit (SPC), and our proposed Strict Imperfection Penalty F1 (SIP-F1). A robust and consistent hierarchy emerges across the entire model spectrum:

$$\text{Score}_{\text{SPC}} > \text{Score}_{\text{SIP-F1}} > \text{Score}_{\text{EM}}. \quad (6)$$

The EM scores (ranging from 0.43 to 0.68) serve as a conservative lower bound, revealing the immense challenge of achieving “perfect alignment” in PhD-level multimodal reasoning. In specialized domains like SPM, a single error in identifying a moiré periodicity or a dI/dV peak leads to a total score of zero in EM, often masking the model’s latent partial understanding. Conversely, SPC provides an optimistic upper bound by measuring “Pure Recall” under the condition of zero-tolerance for errors. However, the most profound scientific insight is found in the gap between SPC and our SIP-F1 metric.

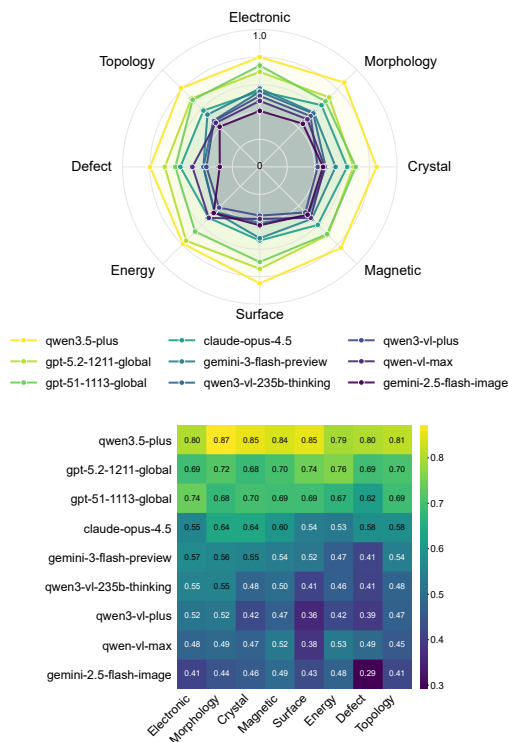


Figure 6: Comparative analysis of model performance in scientific reasoning.

This gap serves as a diagnostic tool for quantifying model “Reasoning Personalities.” Models exhibiting a wide gap, such as *gemini-2.5-flash-image-preview* and *qwen3-vl-plus*, manifest an “Aggressive” or “Gambling” personality. These models tend to over-select options to maximize recall—a behavior we term “speculative hallucination.” In a laboratory setting, such “Gambling Intelligence” is hazardous as it produces false-positive discoveries. In sharp contrast, top-tier models like *gpt-5.2-1211-global* maintain the tightest gap between SPC and SIP-F1. This signifies a “Wise” or “Conservative” profile, characterized by high Epistemic Humility. These models prioritize precision, selecting only the evidence-backed options that can be rigorously synthesized from the complex visual-textual inputs, thus avoiding the devastating $\Gamma = 6$ penalty that SIP-F1 imposes on false positives.

When compared to contemporary scientific benchmarks, the uniqueness of SPM-Bench’s evaluation framework becomes evident. Traditional benchmarks like MMMU [36] and ScienceQA predominantly rely on Exact Match (EM), which fails to distinguish between a “near-miss” and total ignorance. Recent physics-focused datasets such as PhysReason [37] and SEEPHYS [32] have begun to use standard F1-scores, but these metrics are still vulnerable to “gaming” behaviors where models trade precision for recall. As shown in Figure 7, the bimodal distribution induced by SIP-F1 creates a “Scientific Reasoning Barrier” that standard F1 cannot capture. While SuperGPQA [5] targets PhD-level knowledge, it remains a text-centric or descriptive-heavy evaluation. SPM-Bench, through its integration of SIP-F1, is the first to transform benchmarking

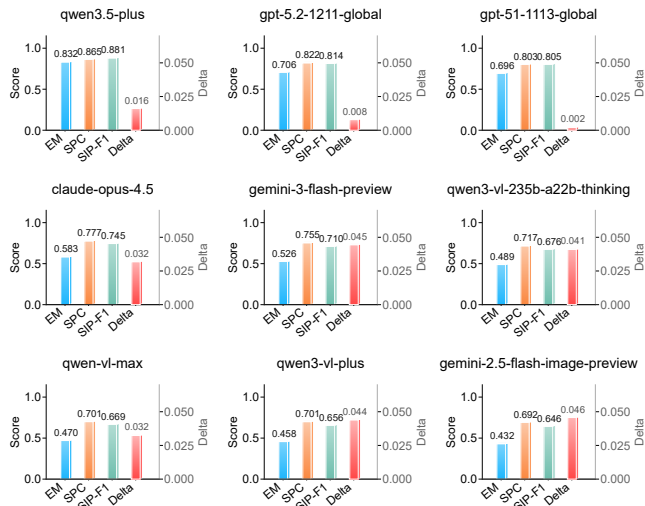


Figure 7: Analysis of accuracy under EM, SPC, and SIP-F1 evaluation metrics.

from a simple “test of knowledge” into a “stress test of scientific integrity,” ensuring that AI agents are evaluated not just on their ability to find the right answer, but on their reliability in rejecting the wrong ones.

4.2 Behavioral Personality

Figure 8 provides a multidimensional analysis of SOTA model performance by correlating reasoning robustness (SIP-F1) with three meta-behavioral indicators: model-reported confidence, perceived task difficulty, and generation efficiency (Average Tokens). This holistic view allows us, for the first time, to transcend beyond mere accuracy scores and profile the “Behavioral Personalities” of state-of-the-art LLMs in specialized scientific environments [15, 16, 40].

Overconfidence and Reliability A critical highlight of our study is the exposure of the “Overconfidence Gap,” primarily manifest in models like *gemini-3-flash-preview*. Despite reporting the highest self-confidence (~ 0.90), its SIP-F1 (0.71) significantly lags behind the frontier, revealing a personality we define as the aggressive personality. Scientifically, this misalignment suggests a failure in *metacognitive calibration*: the model generates authoritative, expert-sounding physical explanations while lacking the underlying logical integrity to ensure their validity. This “Epistemic Hubris” is particularly hazardous in surface physics; for instance, confidently misidentifying a Friedel oscillation as a covalent bond can lead to erroneous structural models.

In sharp contrast, the wise personality (exemplified by the *gpt-5* series) is characterized by a high correlation between perceived difficulty and confidence. These models exhibit a sophisticated awareness of their own knowledge boundaries, lowering their confidence when confronted with complex scenarios such as FFT analysis of disordered lattices. This calibrated self-awareness transforms them from mere black-box predictors into reliable scientific collaborators.

Most strikingly, the introduction of *qwen3.5-plus* redefines the performance ceiling of this benchmark. It achieves a breakthrough Exact Match (EM) of 0.832 and an unprecedented SIP-F1 score of 0.881, significantly outpacing the frontier *gpt-5* series. Crucially, its Delta gap between SPC and SIP-F1 is a mere 0.016. This microscopic penalty indicates that despite its exceptionally high recall, it produces virtually zero hallucinatory false-positives. *qwen3.5-plus* proves that absolute supremacy in PhD-level SPM reasoning is achievable when a model successfully marries the "Wise" conservative selection strategy with an vastly expanded scientific knowledge base, effectively eliminating the trade-off between recall and precision.

Logical Depth and Token Efficiency We observe a clear trade-off between output conciseness and reasoning integrity. Models like *qwen-vl-max* represent the "Naive Intuitionist" profile—producing rapid, low-token responses that are adequate for Level-1 observational tasks but collapse under Level-5 evaluative reasoning. Our findings indicate that scientific robustness in the physical sciences is intrinsically tied to the "depth of pondering"; without sufficient token-space to traverse the latent physical constraints of a problem, models inevitably resort to shallow heuristics, further justifying the necessity of the SIP-F1 penalty for punishing such speculative shortcuts.

Behavioral Personality Profiling The "Aggressive" profile, exemplified by *gemini-3-flash-preview*, manifests significant "Epistemic Hubris," reporting extreme self-confidence (~0.90) despite a massive token expenditure (~4,077) that fails to translate into a frontier-level SIP-F1 (0.710), suggesting that verbosity without calibration often leads to speculative shortcuts. In contrast, *qwen3.5-plus* with "Wise" personality reports an extremely high confidence (~0.935) and consumes the highest token volume across the entire spectrum (4,890 tokens), yet it perceives the task difficulty as significantly high (0.773). Unlike *gemini-3-flash-preview*, where high token usage translates to "Epistemic Hubris" and speculative errors, *qwen3.5-plus* converts its massive computational expenditure into flawless reasoning (SIP-F1 0.881). It demonstrates that in complex physical sciences, verbosity is not inherently detrimental if it is heavily anchored in rigorous, step-by-step physical deduction. Its high confidence is not an illusion but a fully calibrated reflection of its absolute domain mastery. The *gpt-5* series achieves the performance ceiling through superior metacognitive calibration, maintaining a tight alignment between perceived difficulty and confidence. Most notably, the "Deliberative Analyst" profile, represented by *qwen3-vl-235b-a22b-thinking*, utilizes test-time reasoning scaling to prioritize logical integrity over output conciseness. For this model, the substantial token overhead (~3,203) is not a sign of inefficiency but serves as an explicit computational workspace to externalize and verify the latent physical constraints of the SPM domain. By transforming internal Chain-of-Thought (CoT) into a complete, transparent derivation, this personality ensures that scientific robustness is anchored in a rigorous "System 2" traversal of the problem space rather than the shallow heuristics of the "Naive Intuitionist" (e.g., *qwen-vl-max*).

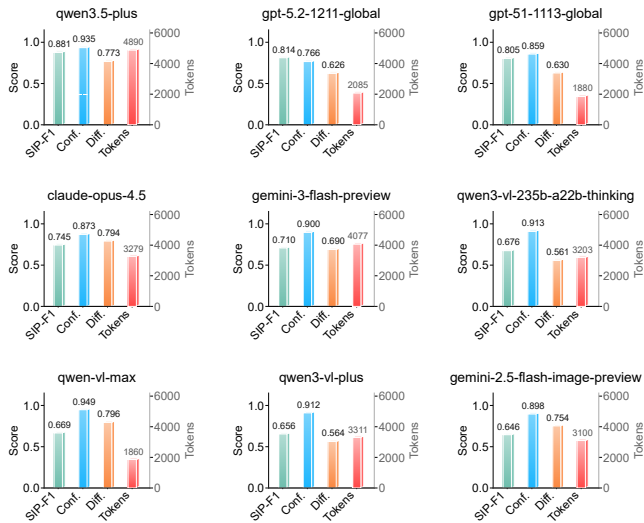


Figure 8: Comparison of model confidence, difficulty and tokens.

4.3 Domain Expertise

Figure 6 dissects model performance across eight specialized scientific domains. The radar charts visualize the **competence envelope** for each model family, revealing a clear distinction between basic visual perception and advanced physical deduction.

Qwen’s Dominant Performance. The most striking observation is the comprehensive superiority of *qwen3.5-plus* (yellow polygon), which encloses all other models across every domain. Unlike previous iterations where Qwen models lagged behind GPT series in scientific reasoning, *qwen3.5-plus* achieves unprecedented scores in *Morphology and Composition Analysis* (0.87) and *Surface Chemical Reactions* (0.85). This suggests a fundamental breakthrough in the model’s ability to correlate macroscopic visual features with microscopic physical laws. Notably, even in traditionally challenging domains like *Electronic Structure* (0.80) and *Energy Materials* (0.79), *qwen3.5-plus* maintains a significant lead over *gpt-5.2-1211-global* (0.69 and 0.76, respectively), indicating that the new architecture has successfully internalized complex quantum-mechanical concepts rather than relying on superficial pattern matching.

Generational Leap and Reasoning Scaling. Comparing *qwen3.5-plus* with its predecessor *qwen-vl-max* reveals the impact of reasoning-oriented scaling. While *qwen-vl-max* struggles in abstract domains like *Defect Engineering* (0.49) and *Topology* (0.45), the newer version improves these scores by approximately 60% (to 0.80 and 0.81). This "area expansion" in the radar plot confirms that increasing parameter count and optimizing for Chain-of-Thought (CoT) reasoning allows the model to better parse the spatial hierarchy of scientific figures, leading to a more accurate mapping of visual evidence to physical laws. Similarly, the **Gemini family** exhibits a noticeable generational leap; *Gemini-3-flash-preview* significantly expands its reasoning radius in *Electronic Structure* (0.57) compared to the 0.41 achieved by *Gemini-2.5-flash-image*, suggesting a transition from surface-level recognition to semantic understanding.

Universal Bottlenecks in Quantum Domains. Despite the general progress, specific "blind spots" persist across all model families. *Defect Engineering and Property Modulation* remains the most formidable bottleneck, with scores typically 10–15% lower than those in *Morphology Analysis*. For instance, even the top-performing *qwen3.5-plus* sees a dip to 0.79 in *Energy* and 0.80 in *Electronic*, while lower-tier models like *gemini-2.5-flash-image* collapse to 0.29 in *Defect*. This is likely because characterizing defects (e.g., atomic vacancies or dopants) requires the model to interpret "imperfections" against a theoretically perfect lattice, demanding a higher-order dual-task reasoning that most VLMs still struggle to coordinate. Such a gap implies that while pre-training data is abundant in ideal crystal structures, it lacks the deep logical scaffolding for non-ideal symmetry breaking.

Intra-family Evolutionary Refinement While the gap between general-purpose VLMs and PhD-level physics remains significant, our results highlight a steady evolutionary trajectory within model families. In the **Qwen family**, *qwen3-vl-235b-thinking* shows a consistent margin over *qwen3-vl-plus* in domains requiring structural logic, such as *Surface Chemical Reactions* (0.4091 vs. 0.3551) and *Crystal Structure Analysis* (0.4808 vs. 0.4224). Similarly, the **Gemini family** exhibits a noticeable leap; *Gemini-3-flash-preview* significantly expands its "reasoning radius" in *Electronic Structure and Surface States* (0.5714) compared to the 0.4086 achieved by *Gemini-2.5-flash-image-preview*. This suggests that recent iterations are successfully transitioning from "surface-level pattern matching" to a more nuanced understanding of reciprocal space and symmetry-breaking events.

Heterogeneous Knowledge Distribution and Universal Bottlenecks. The radar charts expose specific "blind spots" shared by most models. For instance, *Defect Engineering and Property Modulation* remains the most formidable bottleneck across all three families, with scores typically 10–15% lower than those in *Morphology Analysis*. This is likely because characterizing defects (e.g., atomic vacancies or dopants) requires the model to interpret "imperfections" against a theoretically perfect lattice, demanding a higher-order dual-task reasoning that most VLMs still struggle to coordinate. Such a gap implies that while pre-training data is abundant in ideal crystal structures, it lacks the deep logical scaffolding for non-ideal symmetry breaking, thereby hindering the models' ability to generalize across these structural outliers.

In contrast, all models perform relatively well in *Morphology and Composition Analysis*, suggesting that basic shape recognition presents a lower entry barrier for all models [12]; however, the performance ceiling in these perceptual tasks remains unexpectedly decoupled from the scaling of reasoning capabilities. The real frontier, as evidenced by the "spiky" profiles of the Qwen and Gemini series, lies in bridging the gap between "seeing" a cluster and "calculating" its quantum implications—a domain where only the top-tier GPT series currently exhibits stable competence. Figure 6 dissects model performance across eight specialized scientific domains. The radar charts visualize the **competence envelope** for each model family, revealing a clear distinction between basic visual perception and advanced physical deduction.

In summary, we introduce SPM-Bench to stress-test MLLM reasoning in physical sciences. Our work offers three contributions:

Automated Data Synthesis We developed a near-zero-human pipeline to decouple visual evidence from textual noise, producing 2,703 PhD-level questions grounded in pure visual-physical signals.

A Rigorous Evaluative Metric (SIP-F1) We propose the Strict Imperfection Penalty F1 (SIP-F1) score. Unlike traditional metrics, SIP-F1 strictly penalizes hallucinations and gambling behaviors, prioritizing scientific integrity over simple accuracy.

Behavioral Personality Profiling We diagnose LLM "Scientific Personalities," revealing a critical gap between the epistemic humility of frontier models and the speculative aggression of others. This highlights the necessity of metacognitive calibration in AI.

Ultimately, SPM-Bench demonstrates that in scientific domains, metrics are as important as data. By shifting focus from raw performance to behavioral reliability, we ensure AI agents serve as trustworthy collaborators in discovery.

References

- [1] Shuai Bai, Keqin Chen, et al. 2025. Qwen2.5-VL Technical Report. *arXiv preprint arXiv:2502.13923* (2025).
- [2] John Canny. 1986. A computational approach to edge detection. *IEEE Transactions on Pattern Analysis and Machine Intelligence* 6 (1986), 679–698.
- [3] Jiaze Chen, Tiantian Fan, et al. 2025. Seed1.5-thinking: Advancing Superb Reasoning Models with Reinforcement Learning. *arXiv preprint arXiv:2504.13914* (2025).
- [4] X. Dai et al. 2025. PHYSICSARENA: A Multimodal Physics Reasoning Benchmark Exploring Variable, Process, and Solution Dimensions. *arXiv preprint arXiv:2505.15472* (2025).
- [5] Xinrun Du, Yifan Yao, et al. 2025. SuperGPQA: Scaling LLM Evaluation Across 285 Graduate Disciplines. *arXiv preprint arXiv:2502.14739* (2025).
- [6] Richard O Duda and Peter E Hart. 1972. Use of the Hough transformation to detect lines and curves in pictures. *Commun. ACM* 15, 1 (1972), 11–15.
- [7] Jingxuan Fan et al. 2024. Hardmath: A Benchmark Dataset for Challenging Problems in Applied Mathematics. *arXiv preprint arXiv:2410.09988* (2024).
- [8] Lloyd Alan Fletcher and Rangachar Kasturi. 1988. A robust algorithm for text string separation from mixed text/graphics images. *IEEE Transactions on Pattern Analysis and Machine Intelligence* 10, 6 (1988), 910–918.
- [9] Bofei Gao, Feifan Song, et al. 2025. Omni-math: A Universal Olympiad Level Mathematic Benchmark for Large Language Models. In *The Thirteenth International Conference on Learning Representations (ICLR)*.
- [10] Yuchao Gu et al. 2024. AstroMMBench: A Benchmark for Evaluating Multimodal Large Language Models Capabilities in Astronomy. *arXiv preprint arXiv:2410.00063* (2024).
- [11] Daya Guo, Dejian Yang, et al. 2025. DeepSeek-R1: Incentivizing Reasoning Capability in LLMs via Reinforcement Learning. *arXiv preprint arXiv:2501.12948* (2025).
- [12] Yunzhuo Hao, Jiawei Gu, Huichen Will Wang, Linjie Li, Zhengyuan Yang, Lijuan Wang, and Yu Cheng. 2025. Can MLLMs Reason in Multimodality? EMMA: An Enhanced MultiModal Reasoning Benchmark. *arXiv:2501.05444 [cs.CV]* <https://arxiv.org/abs/2501.05444>
- [13] Chaoqun He, Renjie Luo, et al. 2024. OlympiadBench: A Challenging Benchmark for Promoting AGI with Olympiad-Level Bilingual Multimodal Scientific Problems. In *Proceedings of the 62nd Annual Meeting of the Association for Computational Linguistics (ACL)*. 3828–3850.
- [14] Dan Hendrycks, Collin Burns, et al. 2021. Measuring Massive Multitask Language Understanding. In *Proceedings of the International Conference on Learning Representations (ICLR)*.
- [15] Guangyuan Jiang, Manjie Xu, Song-Chun Zhu, Wenjuan Han, Chi Zhang, and Yixin Zhu. 2023. Evaluating and inducing personality in pre-trained language models. In *Proceedings of the 37th International Conference on Neural Information Processing Systems (New Orleans, LA, USA) (NIPS '23)*. Curran Associates Inc., Article 466, 22 pages.
- [16] Saurav Kadavath, Tom Conerly, Amanda Askell, et al. 2022. Language Models (Mostly) Know What They Know. *arXiv:2207.05221 [cs.CL]* <https://arxiv.org/abs/2207.05221>
- [17] Manyu Li et al. 2025. MicroVQA++: High-Quality Microscopy Reasoning Dataset with Weakly Supervised Graphs for Multimodal Large Language Model. *arXiv preprint arXiv:2511.11407* (2025).
- [18] Percy Liang, Rishi Bommasani, Tony Lee, et al. 2023. Holistic Evaluation of Language Models. *Transactions on Machine Learning Research* (2023). <https://openreview.net/forum?id=iO4LZibEqW>

- [19] Junqi Liu, Jonas Bayer, Xiaodan Liang, et al. 2025. CombiBench: Benchmarking LLM Capability for Combinatorial Mathematics. *arXiv preprint arXiv:2501.11284* (2025).
- [20] Yang Liu, Dan Iter, Shuo Xu, et al. 2023. G-eval: NLG evaluation using gpt-4 with better human alignment. *arXiv preprint arXiv:2303.16634* (2023).
- [21] LINHAO LUO, Yuan-Fang Li, Gholamreza Haffari, and Shirui Pan. 2024. Reasoning on Graphs: Faithful and Interpretable Large Language Model Reasoning. (2024). <https://openreview.net/forum?id=ZGNWW7xZ6Q>
- [22] L. O’Gorman. 1993. The document spectrum for page layout analysis. *IEEE Transactions on Pattern Analysis and Machine Intelligence* 15, 11 (1993), 1162–1173. doi:10.1109/34.244677
- [23] Long Phan et al. 2025. Humanity’s Last Exam. *arXiv preprint arXiv:2501.14249* (2025). <https://arxiv.org/pdf/2501.14249>
- [24] Hui Shen et al. 2025. PHYX: Does Your Model Have the “Wits” for Physical Reasoning? *arXiv preprint arXiv:2502.15929* (2025).
- [25] Qianwen Shen, Zeyu Ma, and Mingang Chen. 2025. *From Chart to QA Pairs: A Context-Aware Generation Framework for Chart-Containing Documents*. Association for Computing Machinery, 101–107. <https://doi.org/10.1145/3728725.3728741>
- [26] Aarush Sinha, OmKumar Chandra Umakanthan, and Sudhakaran Gajendran. 2025. DR-CoT: dynamic recursive chain of thought with meta reasoning for parameter efficient models. *Scientific Reports* 15, 1 (2025), 4125. <https://doi.org/10.1038/s41598-025-18622-6>
- [27] Karl Tombre, Christian Ah-Soon, Philippe Dosch, Gerald Masini, and Salvatore Tabbone. 2002. Text/graphics separation revisited. In *Workshop on Document Analysis Systems*. Springer, 1–12.
- [28] Xuezhong Wang, Jason Wei, Dale Schuurmans, Quoc Le, Ed Chi, Sharan Narang, Aakanksha Chowdhery, and Denny Zhou. 2023. Self-Consistency Improves Chain of Thought Reasoning in Language Models. *arXiv:2203.11171 [cs.CL]* <https://arxiv.org/abs/2203.11171>
- [29] Jason Wei, Xuezhong Wang, Dale Schuurmans, et al. 2022. Chain-of-thought prompting elicits reasoning in large language models. *Advances in Neural Information Processing Systems* 35 (2022), 24824–24837.
- [30] Yonghao Weng et al. 2025. MatQnA: A Benchmark Dataset for Multi-modal Large Language Models in Materials Characterization and Analysis. *arXiv preprint arXiv:2509.11335* (2025).
- [31] Hjalmar Wijk, Tao Lin, Joel Becker, Sami Jawhar, Neev Parikh, Thomas Broadley, Lawrence Chan, Michael Chen, Josh Clymer, Jai Dhyani, Elena Ericheva, Katharyn Garcia, Brian Goodrich, Nikola Jurkovic, Holden Karnofsky, Megan Kinniment, Aron Lajko, Seraphina Nix, Lucas Sato, William Saunders, Maksym Taran, Ben West, and Elizabeth Barnes. 2025. RE-Bench: Evaluating frontier AI&D capabilities of language model agents against human experts. *arXiv:2411.15114 [cs.LG]* <https://arxiv.org/abs/2411.15114>
- [32] Kun Xiang, Heng Li, Xiaodan Liang, et al. 2025. SEEPHYS: Does Seeing Help Thinking? – Benchmarking Vision-Based Physics Reasoning. *arXiv preprint arXiv:2505.19099* (2025).
- [33] Xin Xu et al. 2025. UGPhysics: A Comprehensive Benchmark for Undergraduate Physics Reasoning with Large Language Models. *arXiv preprint arXiv:2502.00334* (2025).
- [34] An Yang et al. 2024. Qwen2.5-Math Technical Report: Toward Mathematical Expert Model via Self-improvement. *arXiv preprint arXiv:2409.12122* (2024).
- [35] Junchi Yu, Ran He, and Zhitao Ying. 2024. Thought propagation: An analogical approach to complex reasoning with large language models. (2024). <https://openreview.net/forum?id=SB0RhRCzM3>
- [36] Xiang Yue, Yuansheng Ni, et al. 2024. MMMU: A Massive Multi-discipline Multi-modal Understanding and Reasoning Benchmark for Expert AGI. In *Proceedings of the IEEE/CVF Conference on Computer Vision and Pattern Recognition (CVPR)*.
- [37] Xinyu Zhang et al. 2025. PhysReason: A Comprehensive Benchmark towards Physics-Based Reasoning. *arXiv preprint arXiv:2502.12054* (2025).
- [38] Yaowei Zheng et al. 2024. LlamaFactory: Unified Efficient Fine-Tuning of 100+ Language Models. *arXiv preprint arXiv:2403.13372* (2024).
- [39] Wanjun Zhong et al. 2023. AGIEval: A Human-Centric Benchmark for Evaluating Foundation Models. *arXiv preprint arXiv:2304.06364* (2023).
- [40] Minjun Zhu, Yixuan Weng, Linyi Yang, and Yue Zhang. 2025. Personality Alignment of Large Language Models. (2025). <https://openreview.net/forum?id=0DZEs8NpUH>

A Details in SPM-Bench

As illustrated in Figure 1 and detailed in Table 1, SPM-Bench comprises 2,703 high-quality multimodal questions, each paired with a unique, high-resolution microscopy image. The dataset maintains a robust balance across four pillar characterization techniques: Transmission Electron Microscopy (TEM, $n = 955$), Scanning Tunneling Microscopy (STM, $n = 752$), Scanning Electron Microscopy (SEM, $n = 558$), and Atomic Force Microscopy (AFM, $n = 438$). This distribution ensures that the benchmark covers a broad spectrum of spatial scales and physical observables, ranging from the atomic-scale electronic density of states (LDOS) in STM to the mesoscopic morphological features and phase transitions in SEM.

Taxonomic Hierarchy and Semantic Coverage. The sunburst chart in Figure 1 reveals the multi-layered taxonomic structure of SPM-Bench. Beyond the primary imaging modalities, the dataset is systematically organized into specialized physical domains such as *Electronic Structure*, *Magnetic Materials*, *Topological Insulators*, and *Surface Engineering*. The outermost ring highlights the "PhD-level" granularity of the benchmark, encompassing high-entropy scientific concepts including the *Rashba Effect*, *Van Hove Singularities*, *Charge Density Waves (CDW)*, and *Skymion Lattice* configurations. This dense semantic coverage ensures that a model cannot solve SPM-Bench through simple pattern matching; instead, it must perform rigorous cross-modal reasoning between subtle visual features and fundamental physical laws.

Information Density and Complexity. Table 1 further underscores the linguistic and reasoning complexity of the benchmark. The average prompt length stands at 3,393.4 tokens, indicating that each question is embedded in a rich, context-heavy environment synthesized from original arXiv and journal publications. Furthermore, the average output length of 1,266.0 tokens signifies that the tasks are specifically designed to elicit long-form, analytical reasoning (Chain-of-Thought) rather than brief, superficial answers. By integrating peer-reviewed data from over 825 unique scientific papers (407 from arXiv and 418 from high-impact journals), SPM-Bench provides a high-fidelity "academic purity" that effectively minimizes the risk of data contamination common in general-purpose web-crawled datasets.

To benchmark the cognitive maturity of LLMs, we categorize SPM-Bench into five hierarchical levels based on Bloom’s Taxonomy, mapping tasks from basic perception to advanced scientific synthesis: Level 1 - Recall & Recognition; Level 2 - Comprehension; Level 3 - Application; Level 4 - Analysis; Level 5 - Evaluation & Synthesis.

Level 1 - Recall & Recognition: Identification of fundamental imaging modalities or prominent surface features. *E.g.*, "Is this image acquired via STM or nc-AFM based on the contrast mechanism?"

Level 2 - Comprehension: Interpretation of localized visual signals within a physical context. *E.g.*, "What does the bright protrusion at the center of the hexagonal lattice represent (e.g., a single adatom or a vacancy)?"

Level 3 - Application: Utilizing physical laws or structural parameters to derive specific properties. *E.g.*, "Calculate the moiré periodicity and determine the corresponding twist angle between the layers."

Table 3: Taxonomy and Comparison of Emerging Scientific Reasoning Benchmarks.

Benchmark	Time	Mod.	Num.	Area	Type
SPM-Bench	Feb-26	MM	2.7k	Phys. Mat.	MCQ, VQA
MicroVQA++	Nov-25	MM	26k	Bio.	MCQ, VQA
AstroMMBench	Oct-25	MM	621	Astro.	MCQ
AMO-Bench	Oct-25	TXT	50	Math.	OE, Calc.
MatSciBench	Oct-25	MM	1.3k	Mat. Sci.	OE, Calc.
SEEPHYS	Oct-25	MM	2k	Phys.	OE, Reas.
MatQnA	Sep-25	MM	5k	Mat.	MCQ, Sub.
Multi-Physics	Sep-25	MM	1.4k	Phys.	MCQ, VQA
CMPhysBench	Aug-25	TXT	520	Phys.	OE, Calc.
DeepPHY	Aug-25	MM	1.3k	Phys.	VQA, Reas.
PhysUniBench	Jun-25	MM	3.3k	Phys.	OE, MCQ
UGPhysics	Jun-25	TXT	5.5k	Phys.	OE, Reas.
PHYBench	May-25	TXT	500	Phys.	Calc. Reas.
MicroVQA	Mar-25	MM	1k	Bio.	MCQ
PhysReason	May-25	MM	1.2k	Phys.	Calc. Reas.
SuperGPQA	Mar-25	TXT	9k	STEM	MCQ
TPBench	Feb-25	TXT	57	Phys. Math.	Reas.
HLE	Jan-25	MM	2.3k	STEM	MCQ, SA
LLM4Mat-Bench	Dec-24	TXT	1.9M	Mat.	OE, Reas.
OlympiadBench	Jun-24	MM	8.5k	Math. Phys.	OE, SA

Abbr: **Mod:** MM (Multimodal), TXT (Text); **Area:** Phys. (Physics), Mat. (Materials), Bio. (Biology), Astro. (Astronomy), Math. (Mathematics); **Type:** MCQ (Multi-Choice), VQA (Visual QA), OE (Open-Ended), Calc. (Calculate), SA (Short-answer), Sub. (Subjective), Reas. (Reasoning).

Level 4 - Analysis: Correlating heterogeneous data streams, such as multi-panel images and spectroscopic mappings. *E.g.*, "Map the dI/dV spectroscopic peaks to specific spatial sites to identify the local density of states (LDOS) modulation."

Level 5 - Evaluation & Synthesis: Critical judgment of physical hypotheses and experimental design. *E.g.*, "Which atomic model best explains the observed symmetry breaking in the topography, and what subsequent experiment would confirm this?"

Besides, to rigorously probe the "reasoning boundaries" of artificial intelligence, SPM-Bench categorizes tasks into a specialized cognitive taxonomy, reflecting the diverse responsibilities of a research scientist as follows: **Expert Visual Understanding (EU)** forces the model to perform quantitative and qualitative decoding of complex visual data; **Hypothesis Generation (HG)** evaluates inductive reasoning; **Experiment Proposal (EP)** tests deductive capability. We present the categorizes in the following appendix section C.

B Sensitivity Analysis of SIP-F1 Metric

To further justify the robustness of our proposed **Strict Imperfection Penalty F1 (SIP-F1)** metric, we provide a quantitative sensitivity analysis across various problem complexities ($|S_c|$), model detection outcomes ($\{TP, FP\}$), and hyperparameter configurations (Γ, λ).

As shown in Table 4, the metric successfully induces a clear bimodal separation between different model "personalities":

- **First Tier (1.00)** Completely correct. Only models with extremely high reasoning capabilities gather in this region.
- **Second Tier (~0.4, Pink)**: Represents the "Conservative" profile, where the model maintains high precision but incomplete recall.
- **Third Tier (~0.25, Blue)**: Represents the "Aggressive" or "Gambling" profile, where correct selections are heavily penalized by the inclusion of hallucinations (FP).

Mathematical Logic of the Bimodal Landscape As evidenced by the shaded regions in Table 4, the SIP-F1 metric induces a sharp scoring gradient that differentiates "cautious knowledge" from "reckless speculation." Under our selected configuration ($\Gamma = 6, \lambda = 0.6$), a model that provides a conservative partial answer (e.g., $|S_c| = 2, \{TP = 1, FP = 0\}$) receives a stable score of **0.400** (Pink Tier). In contrast, an aggressive response that achieves higher recall but includes a single hallucination (e.g., $|S_c| = 2, \{TP = 2, FP = 1\}$) is heavily penalized, dropping the score to **0.240** (Blue Tier). This inverse relationship between recall and score in the presence of false positives effectively prevents the "Reward for Gambling" common in standard F1-metrics, ensuring that the scoring hierarchy remains aligned with scientific integrity.

Impact of the Hallucination Penalty (Γ) The sensitivity of Γ across varied problem complexities ($|S_c| = 1$ to 3) demonstrates its role as an "epistemic filter." As Γ scales from 1 to 10, the scores for any response containing $FP > 0$ exhibit a rapid power-law decay. By setting $\Gamma = 6$, we intentionally create a "Strict Penalty Gap" where the cost of a single error (hallucination) outweighs the benefit of completing the recall. This is particularly visible in the $|S_c| = 3$ case: selecting two correct answers with zero errors yields 0.480, while selecting all three correct answers but including one error ($FP = 1$) results in a significantly lower 0.300. This design forces models to prioritize *Precision* over *Recall*—a core requirement for high-stakes laboratory decision-making.

Invariance Across Complexity Scales A critical observation from Table 4 is the metric's stability across different question densities. Whether a problem requires a single choice ($|S_c| = 1$) or a complex multi-panel synthesis ($|S_c| = 3$), the Second and Third Tiers remain anchored at approximately 0.4 and 0.25, respectively. This invariance ensures that the "Scientific Personality" diagnosis—categorizing models as *Wise*, *Conservative*, or *Aggressive*—is not skewed by the inherent difficulty of the task.

Anti-Gaming Robustness The bottom-most rows of each complexity block highlight the metric's resistance to "gaming the benchmark." For models that adopt a "select-all" strategy (represented by high FP counts), the scores converge toward the baseline as Γ increases. At our chosen $\Gamma = 6$, such behavior is rendered statistically unviable, yielding scores lower than a purely random guess.

Positive Predictive Bias in "Aggressive" Models. Mid-tier models, exemplified by *Gemini-3-flash-preview*, exhibit what we

term a **Positive Predictive Bias**. These models tend to over-select options in multi-select scientific tasks to maximize recall, effectively "gaming" traditional F1 metrics. However, through the lens of SIP-F1, this behavior is exposed as a lack of logical grounding. Statistically, this bias manifests as a misalignment between high self-reported confidence and low precision. In high-stakes physical discovery, such aggressive predicting is hazardous, as it produces false-positive "discoveries" by speculating on ambiguous visual signals.

Epistemic Uncertainty Awareness in "Wise" Models. In contrast, frontier models like the *GPT-5* series demonstrate **High Epistemic Uncertainty Awareness**. These models are not merely "smarter" but are better calibrated; they exhibit a sophisticated ability to quantify the limits of their own knowledge. When faced with high-entropy physical scenarios (e.g., symmetry-breaking in disordered lattices), they adopt a **Conservative Strategy**, prioritizing precision over speculative recall. This behavior reflects a deep logical internal consistency, where the model's confidence is strongly correlated with the task's intrinsic difficulty. Such models serve as reliable scientific collaborators because they "know when they do not know," thereby minimizing the risk of cascading errors in autonomous research pipelines.

Table 4: Quantitative sensitivity analysis of the SIP-F1 metric across varied problem complexities ($|S_c|$), detection outcomes ($\{TP, FP\}$), and parameter configurations (Γ, λ). Highlighted cells distinguish performance tiers: blue indicates scores approximately at 0.25 (Third Tier), while pink indicates scores approximately at 0.4 (Second Tier).

$ S_c $	$\{TP, FP\}$	Γ	$\lambda = 0.3$	0.4	0.5	0.6	0.7	0.8		
1	{1, 1}	1	0.200	0.267	0.333	0.400	0.467	0.533		
		2	0.150	0.200	0.250	0.300	0.350	0.400		
		4	0.100	0.133	0.167	0.200	0.233	0.267		
		6	0.075	0.100	0.125	0.150	0.175	0.200		
		8	0.060	0.080	0.100	0.120	0.140	0.160		
		10	0.050	0.067	0.083	0.100	0.117	0.133		
		{1, 0}	–	0.200	0.267	0.333	0.400	0.467	0.533	
			1	0.240	0.320	0.400	0.480	0.560	0.640	
		2	{2, 1}	2	0.200	0.267	0.333	0.400	0.467	0.533
				4	0.150	0.200	0.250	0.300	0.350	0.400
6	0.120			0.160	0.200	0.240	0.280	0.320		
8	0.100			0.133	0.167	0.200	0.233	0.267		
10	0.086			0.114	0.143	0.171	0.200	0.229		
{2, 0}	–			0.240	0.320	0.400	0.480	0.560	0.640	
	{1, 0}			–	0.150	0.200	0.250	0.300	0.350	0.400
3	{3, 1}			1	0.257	0.343	0.429	0.514	0.600	0.686
		2	0.214	0.286	0.357	0.429	0.500	0.571		
		4	0.180	0.240	0.300	0.360	0.420	0.480		
		6	0.150	0.200	0.250	0.300	0.350	0.400		
		8	0.130	0.173	0.217	0.261	0.304	0.348		
		10	0.113	0.150	0.188	0.225	0.263	0.300		

C Model Performance Across Different Domains

Deduction Beyond Perception An intriguing observation arises from the performance distribution of the frontier *gpt-5.2-1211-global*. Its peak performance is achieved in *Energy Materials* (0.7600) and *Surface Chemical Reactions* (0.7429)—domains that demand rigorous causal reasoning and the synthesis of multi-panel data (e.g., correlating STM topography with local spectroscopy). In contrast, its score in *Morphology Analysis* (0.7156) is relatively lower, despite this being a more inherently visual” task. This suggests that the scaling of large multimodal models primarily augments their **scientific deductive reasoning** rather than their raw visual acuity. The model is no longer merely recognizing” a cluster; it is “calculating” its structural and chemical implications through an internal physics-aligned logic.

Stability in Frontier Competence As visualized in Figure 8, the *gpt-5* series exhibits an almost perfect circular” profile at high radii. This represents a state of **balanced expert capability**, where the model performs consistently across disparate fields, from *Magnetic Materials* (0.7013) to *Electronic Structure* (0.6929). In sharp contrast, mid-tier models like *Gemini-2.5-flash* and *qwen3-vl-plus* show significantly spiky” or restricted envelopes. These models frequently collapse in high-abstraction domains like *Defect Engineering*, where identifying an atomic vacancy or a dopant site (scoring as low as 0.2917 for *Gemini-2.5*) requires the model to deduce symmetry-breaking rules from subtle contrast variations—a task that remains a definitive bottleneck for VLMs lacking sufficient reasoning-optimization.

Bottlenecks in Quantum Domains Despite the general progress, *Topological States and Quantum Materials* remains one of the most formidable domains for all evaluated models. While the mid-tier *qwen3-vl-plus* hovers at a baseline of 0.4712, the frontier *gpt-5.2-1211-global* manages to reach 0.7043. The ability of the top-tier series to maintain scores above 0.70 in this area confirms that sophisticated internal verification and latent physical knowledge are essential for decoding the high-dimensional data inherent in quantum phenomena. However, the persistent gap between *Morphology* and *Defect/Topology* across the entire spectrum highlights that the transition from visual characterization” to quantum state inference” is the primary frontier for the next generation of AI4Science models. The radar charts illustrate a comparative performance analysis of three major Large Language Model (LLM) families—GPT, Gemini, and Qwen—across eight specialized physical science domains. The results reveal distinct patterns in generational scaling, reasoning capabilities, and domain-specific sensitivities.

Impact of Reasoning Mechanisms on Scientific Accuracy The comparison between *qwen3-vl-235b-thinking* and *qwen3-vl-plus* (Bottom) highlights the profound impact of specialized reasoning architectures. The “Thinking” version demonstrates a significant “area expansion” in the radar plot, particularly in the Electronic, Morphology, and Crystal domains. This suggests that the “thinking” (chain-of-thought) mechanism allows the model to better parse the spatial hierarchy of scientific figures, leading to a more accurate mapping of visual evidence to physical laws. Conversely, the Defect and Energy domains remain common bottlenecks, likely due to



Figure 9: Domain-specific competence envelopes across model families.

the inherent complexity of identifying localized irregularities and low-contrast features in microscopy data.

Generational Leap and Perceptual Evolution The Gemini series (Middle) shows the most dramatic generational performance shift. While *Gemini-2.5-flash-image-preview* exhibits a constrained profile centered around 0.2–0.5, *Gemini-3-flash-preview* shows a robust expansion across all axes, nearly doubling the performance in the Electronic and Topology sectors. This leap suggests a fundamental upgrade in the model’s visual encoder, enabling it to transition from basic pattern recognition to a more sophisticated “semantic understanding” of scientific layouts. However, even with this progress, a noticeable “dip” in the Defect axis persists, indicating that characterizing microscopic imperfections remains a cross-model challenge in the current state of VLMs.

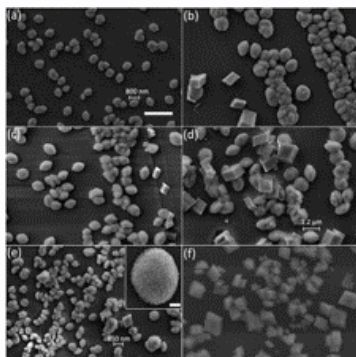
D Typical QA in SPM-Bench

Example 1: SEM

Question: The SEM images in panels (a) through (f) depict the structural evolution of a condensed phase system within a liquid medium. Panel (a) shows the initial dominance of **Phase α** , characterized by a curvilinear morphology. The high-magnification inset in panel (e) reveals the surface topography of **Phase α** entity. As the system evolves toward panel (f), **Phase β** , exhibiting a distinct faceted habit, becomes the sole constituent. Based on the visual evidence provided and the fundamental principles of phase transition kinetics, which of the following statements regarding the observed process are consistent with the visual evidence?

- A. The transition from Phase α to Phase β is a solution-mediated process driven by a chemical potential gradient, where the higher solubility of the metastable Phase α facilitates the nucleated growth of the thermodynamically stable Phase β .
- B. The granular substructure observed in the inset of (e) identifies Phase α as a mesocrystalline assembly of nanocrystalline subunits, indicating a non-classical crystallization pathway involving the oriented attachment of primary particles.
- C. The morphological evolution represents a topotactic solid-state transition, where the faceted geometry in (f) emerges through the collective migration of coherent grain boundaries within the precursor Phase α volume.
- D. The coexistence of Phase α and Phase β in panels (b) through (e) is indicative of a first-order phase transition where the global transformation rate is governed by the competitive rates of dissolution and secondary nucleation.
- E. The transition is a purely curvature-driven Ostwald ripening process within a single-phase system, where the faceted habit in (f) represents the minimization of the surface-to-volume ratio of the initial objects in (a).
- F. The inset in (e) demonstrates that Phase α is an amorphous precursor, and the transition to (f) occurs via a glass-to-crystal transition that bypasses the liquid-phase chemical equilibrium.

Answer: A, B, D



Level: PhD

Discipline: Condensed Matter Physics

Domain: Thermodynamics and Phase Transitions

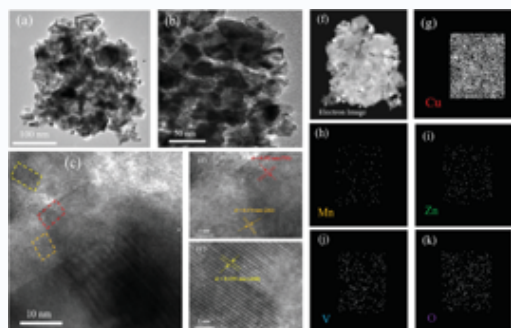
Question Type: HG

Example 2: TEM

Question: A multicomponent inorganic specimen is characterized using various electron-beam modalities in panels (a-k). Panel (f) represents an incoherent imaging mode, while panels (c-e) utilize a coherent phase-contrast mode. Panels (g-k) display the spatial distribution of Species 1-5 (labeled G-K). Based on the visual evidence and the underlying physics of electron-matter interactions, which of the following statements regarding the observed process and data interpretation are consistent with the evidence?

- A. The spatial distribution of Species H and I in panels (h) and (i) indicates preferential segregation at the grain boundaries visible in (b), suggesting a solute-drag mechanism during crystallization.
- B. The intensity variations in the micrograph (f) are purely a function of the atomic number (Z^n) of the constituent species, as the imaging mode effectively filters out all thickness-dependent dynamical diffraction effects.
- C. The contrast in panels (c-e) is governed by the interference of the transmitted and diffracted beams, where the image intensity is a convolution of the specimen's projected potential and the oscillatory Contrast Transfer Function (CTF) of the objective lens.
- D. The measured d -spacings in (d) and (e) (0.174 nm and 0.195 nm) provide sufficient evidence to confirm a transition from a low-symmetry monoclinic phase to a high-symmetry $Fd\bar{3}m$ cubic phase across the entire specimen.
- E. The lower signal-to-noise ratio observed for Species K in panel (k) relative to Species G in (g) is primarily due to the significantly higher X-ray fluorescence yield of light elements compared to transition metals.
- F. Deviations in the lattice periodicities observed in (d) and (e) from those of a stoichiometric reference can be utilized to quantify the local concentration of Species H and I via Vegard's Law, provided the system maintains a homogeneous solid solution.

Answer: C, F



Level: PhD

Discipline: Surface Science

Domain: Nanomaterials Characterization

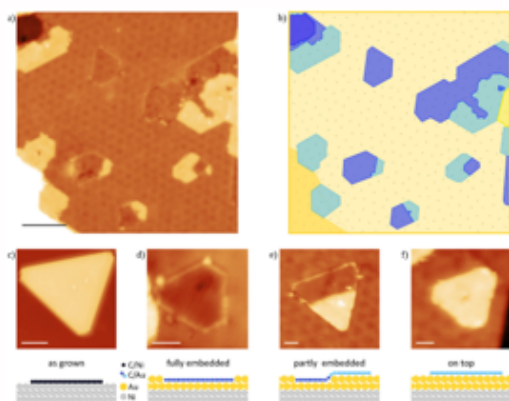
Question Type: EP

Example 3: STM

Question: The provided scanning tunneling microscopy (STM) images (a–f) characterize the structural and electronic evolution of a 2D overlayer (labeled Λ) supported on a metallic substrate (Σ_1) following the introduction of an atomic species (χ). Panel (c) depicts the “as-grown” state of Λ on Σ_1 . Panels (d), (e), and (f) illustrate various stages of the incorporation of χ into the interface. Specifically, panel (e) captures a single domain of Λ spanning two distinct interfacial environments. Based on the visual evidence and the fundamental principles of surface physics, which of the following statements regarding the observed process are consistent with the data?

- The apparent height increase observed in the Λ/χ regions of image (e) is a purely topographic measurement of the χ monolayer thickness, independent of the local tunneling decay constant κ .
- The emergence of the short-period periodic modulation in (f) relative to (c) implies that the lattice mismatch between Λ and the underlying layer increases significantly upon the introduction of χ , as the superlattice periodicity λ is inversely proportional to the mismatch δ .
- The transition from state (c) to (f) signifies an electronic decoupling of Λ from the substrate, shifting the system from a strongly hybridized chemisorbed state to a physisorbed state where the intrinsic electronic structure of the overlayer is largely restored.
- The contrast in (c) is darker than in (f) primarily because the work function (ϕ) of the Λ/Σ_1 interface is significantly higher than that of the $\Lambda/\chi/\Sigma_1$ interface, thereby enhancing the tunneling probability in the latter.
- The spatial configuration in panel (e) demonstrates that the species χ undergoes a surfactant-mediated growth mode, where χ atoms reside exclusively on the exterior surface of Λ to minimize interface energy.
- The visual evidence in (e) and the schematic in (d) confirm that the intercalation of χ is an edge-mediated process, where species χ infiltrates the interface at the boundaries of the Λ domains.

Answer: B, C, F



Level: PhD

Discipline: Condensed Matter Physics

Domain: Graphene Nanoislands

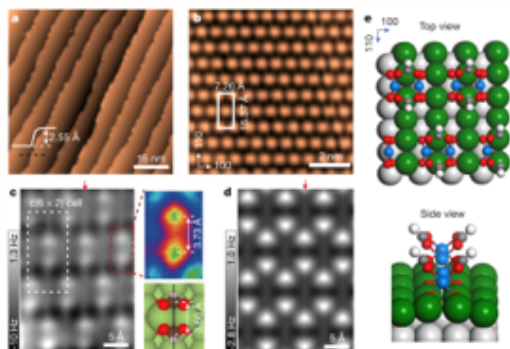
Question Type: EU

Example 4: AFM

Question: The provided figure illustrates the formation of a surface coordination layer on a Cu(110) substrate, characterized by STM (a, b) and nc-AFM (c). Panel (c) displays a frequency shift (Δf) map acquired with a CO-functionalized tip, revealing sub-molecular features within a $c(6 \times 2)$ unit cell. The experimental distance between the prominent bright protrusions is measured at 3.73 Å, which closely matches the 3.66 Å distance between oxygen atoms in the carboxylate ligands shown in the structural model (e). Considering the contrast mechanism in non-contact AFM operating in the repulsive regime with a flexible probe, which of the following statements correctly describes the physical origin of the observed features and the implications for the surface electronic structure?

- A. The bright features in (c) represent the local density of states (LDOS) at the Fermi level, dominated by the metal d -orbitals of the coordination center.
- B. The contrast is primarily governed by Pauli repulsion between the CO tip's frontier orbitals and the electron density of the carboxylate oxygen atoms.
- C. The 3.73 Å distance is a direct measurement of the Cu–Cu distance in the coordination layer, indicating a metallic bond.
- D. The frequency shift Δf is independent of the tip-sample distance in the repulsive regime, allowing for height-independent imaging.
- E. The sub-molecular resolution is a result of the Kondo effect at the metal-organic interface, which enhances the tunneling probability.
- F. The observed contrast arises from the electrostatic attraction between the CO dipole and the partial positive charge on the hydrogen atoms.

Answer: B



Level: PhD

Discipline: Surface Science

Domain: Surface Reconstruction

Question Type: HG